Journal of Colloid and Interface Science **213,** 506–512 (1999)
Article ID jcis.1999.6161, available online at http://www.idealibrary.com on IDEAL®

Nickel Sorption Mechanisms in a Pyrophyllite–Montmorillonite Mixture

Evert J. Elzinga[1] and Donald L. Sparks

Department of Plant and Soil Sciences, University of Delaware, Newark, Delaware 19717-1303

E-mail: elzinga@udel.edu

Received October 6, 1998; accepted February 17, 1999

Nickel sorption on pyrophyllite, montmorillonite and a 1:1 pyrophyllite–montmorillonite mixture was studied at pH 7.5 and a reaction time of 40 min. The main modes of Ni uptake under these reaction conditions are adsorption on montmorillonite and surface precipitation on pyrophyllite. For the clay mixture, where adsorption on the montmorillonite component and surface precipitation on the pyrophyllite component compete for Ni uptake, X-ray absorption fine structure spectroscopy (XAFS) was used to estimate the distribution of Ni over the mixture components. This was done by comparison to pyrophyllite–montmorillonite mixtures with known Ni distributions over the mixture components. Nickel uptake on singly reacted pyrophyllite was slightly higher than on singly reacted montmorillonite. This was consistent with the XAFS results for the clay mixture, which suggested that the pyrophyllite component sorbed slightly more Ni than the montmorillonite component. Our findings suggested that both adsorption and surface precipitation were important mechanisms in the overall Ni uptake in the clay mixture, and that neither sorption mechanism truly out-competed the other in the reaction time of 40 min employed. Therefore, both mechanisms should be considered when modeling Ni sorption in similar systems.

Key Words: **metal sorption; sorption kinetics; XAFS; sorption in sorbent mixtures.**

INTRODUCTION

Experimental studies on metal sorption mechanisms often focus on pure single-mineral sorbents. However, sorbents in natural systems are complex mixtures of a variety of minerals, and as a result, a variety of sorbents will be competing for uptake of metals added to such systems. Therefore, to successfully model and predict the fate of metals in soils and sediments, insight into the competitiveness of available sorption mechanisms is crucial. In this study, we will focus on adsorption and surface precipitation of metals as competing sorption mechanisms at clay mineral surfaces. Adsorption is defined here as a two-dimensional uptake process due to physical and chemical interactions between the metal ion and the clay surface (1). On clay minerals such as montmorillonite adsorption can occur both at the edge sites, which leads to inner-sphere metal complexes, and at the planar (internal) sites of the clay mineral, which results in outer-sphere metal complexes. Recent studies using surface spectroscopic and microscopic techniques such as X-ray absorption fine structure spectroscopy (XAFS), X-ray photo electron spectroscopy (XPS), Auger electron spectroscopy, scanning electron microscopy, atomic force microscopy, and TEM have shown that in many cases the sorption of heavy metals on clay and oxide surfaces results in the formation of three-dimensional multinuclear or polynuclear surface phases (2–10). Such surface phases (surface precipitates) have been observed at surface metal loadings far below a theoretical monolayer, and in a pH range well below the pH where the formation of metal hydroxide precipitates would be expected based on the thermodynamic solubility product (4, 7, 9–12). In the case of Ni sorption on clay mineral surfaces described by Scheidegger *et al.* (10), the surface precipitate was identified as a mixed Ni/Al–hydroxide phase.

It is believed that there is a continuum between Ni adsorption and Ni surface precipitation at clay mineral surfaces. At low surface coverage surface complexation dominates, and as surface coverage increases nucleation occurs and distinct entities or aggregates form at the surface. As surface loading further increases surface precipitation becomes the dominant mechanism (1, 5). Thus, in single mineral sorption systems, surface precipitation and adsorption are thought to be consecutive metal uptake mechanisms. Adsorption is most likely the mechanism responsible for the initial fast stage of Ni sorption, and surface precipitation appears to be an important mechanism controlling the slower stage of Ni uptake.

Time-resolved XAFS studies of Ni sorption on pyrophyllite, montmorillonite, and gibbsite, presented by Scheidegger *et al.* (10), showed that the initiation of mixed Ni/Al–hydroxide surface precipitate formation varies as a function of sorbent type. For example, 40 min after Ni addition, the Ni/montmorillonite system was still in the initial stage of Ni uptake (adsorption), while in the Ni/pyrophyllite system surface precipitate formation had begun after 15 min, and continued rapidly up to about 3 h after Ni addition. The sorbed amount of Ni expressed on a mass basis in both systems was about the same after 40 min. An interesting consequence is that, in a pyrophyllite–montmorillonite mixture, it may be possible to

[1] To whom correspondence should be addressed.

0021-9797/99 $30.00

distinguish between Ni sorption on the montmorillonite and pyrophyllite surfaces using XAFS spectroscopy. Studies on Ni sorption in such a system may give insight as to the sorption of Ni on either surface. XAFS may be a valuable tool in studying such systems, since it can distinguish between adsorption and surface precipitation. Surface precipitation is indicated by the presence of a second neighbor Ni–Ni/Al peak in the radial structure function (RSF) derived from XAFS data, while this peak is absent when adsorption is the main mode of Ni uptake (10, 13). Therefore, in a mixture of montmorillonite and pyrophyllite, where surface precipitation occurs on the pyrophyllite phase and adsorption on the montmorillonite phase, the second Ni–Ni/Al peak in the RSF can be used to distinguish between Ni surface precipitation on pyrophyllite and Ni adsorption on montmorillonite. The intensity of the Ni–Ni/Al peak in the RSF is related to the loading of surface precipitates at the mineral surface. We hypothesize that since the intensity of the Ni–Ni/Al peak will be a function of the Ni loading on pyrophyllite, it can be used to estimate the distribution of Ni in a pyrophyllite/montmorillonite mixture.

The objectives of this study were (1) to characterize Ni sorption in a pyrophyllite/montmorillonite mixture; and (2) to quantify the distribution of Ni between the mineral components of a pyrophyllite/montmorillonite mixture using XAFS.

MATERIALS AND METHODS

The preparation and characterization of the pyrophyllite and montmorillonite clay minerals used in this study are described in Scheidegger *et al.* (9, 10). The specific surface areas of the materials were determined by both the N_2-BET and the ethylene glycol monoethyl ether (EGME) methods. The surface areas were 96 $m^2\ g^{-1}$ (BET) and 95 $m^2\ g^{-1}$ (EGME) for pyrophyllite, and 15.2 $m^2\ g^{-1}$ (BET) and 697 $m^2\ g^{-1}$ (EGME) for montmorillonite. The BET method accounts for the external surface area of the minerals, whereas the EGME method accounts for the external and internal surface area. For montmorillonite, which is a swelling clay mineral, the difference between the EGME and BET surface areas was large, which demonstrates the large internal surface area associated with this clay mineral. For pyrophyllite the variation between the two methods was small, which indicates that no significant amount of swelling clays, such as montmorillonite, was present.

Figure 1 depicts a schematic outline of the methods used in this study. The general procedure employed was to prepare a "reacted mixture" and a number of "standard mixtures," and to compare the XAFS data of the reacted mixture versus the standard mixtures. As shown in Fig. 1, the reacted mixture was prepared by reacting Ni with a clay suspension consisting of both pyrophyllite and montmorillonite, while the standard mixtures were prepared by mixing pyrophyllite and montmorillonite phases that had separately been reacted with Ni. All mixtures consisted of montmorillonite and pyrophyllite mixed in a 50%–50% dry weight ratio, and had a total Ni loading of 3000 mg kg^{-1}. We assume that the onset of surface precipitation at a mineral surface is dictated by the surface loading, as suggested by Fendorf and Sparks (5). Under the same set of reaction conditions (reaction pH 7.5, 0.1 M $NaNO_3$ background electrolyte, initial Ni concentration = 2.3 mM) pyrophyllite and montmorillonite reach the same Ni loading level after a reaction time of 40 min and at a solids concentration of 10 g L^{-1}. This loading level, expressed on a dry mass basis, is 6000 mg kg^{-1}. Preliminary studies indicated that pyrophyllite shows surface precipitation at Ni loading levels as low as 1500 mg kg^{-1} already, and it therefore is well into the stage of surface precipitation at a Ni loading of 6000 mg kg^{-1}. Montmorillonite, on the other hand, is still in the stage of adsorption at a loading level of 6000 mg kg^{-1}. In the most extreme case, Ni added to a mixture of pyrophyllite and montmorillonite will partition to only one surface. In a 50–50 wt% mixture of pyrophyllite and montmorillonite, a 6000 mg kg^{-1} Ni loading on one component and a 0 ppm Ni loading on the other component results in a total Ni loading of 3000 mg kg^{-1} for the mixture as a whole. Since pyrophyllite is already well into the stage of surface precipitation at a surface loading of 6000 mg kg^{-1}, whereas montmorillonite is still in the stage of adsorption at this surface loading, we used total mixture loadings of 3000 mg kg^{-1}.

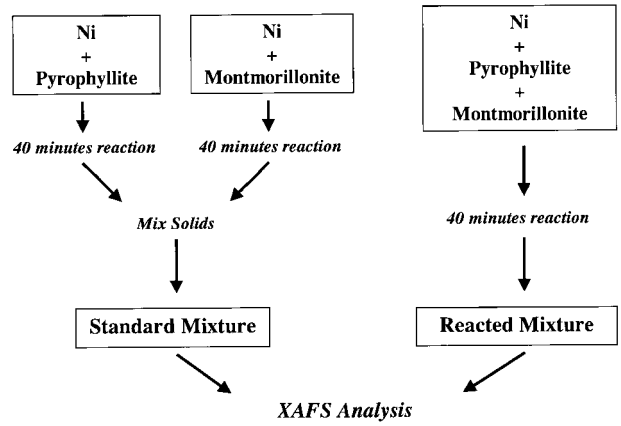

FIG. 1. Schematic outline of the methods used in this study.

Five standard mixtures with a total Ni loading of 3000 mg kg^{-1} but with different distributions of Ni over the pyrophyllite and montmorillonite components were prepared (Table 1). To achieve the Ni sorption levels on the standard mixture components presented in Table 1, the initial Ni concentrations (only montmorillonite) and the solid concentrations (both pyrophyllite and montmorillonite) were varied, while all other experimental conditions that affect the Ni surface loading (pH, background electrolyte, and reaction time) were kept the same. The values of the initial Ni concentrations and solid concentrations used for preparation of the mixture components are given in Table 1. Solution speciation calculations performed with MINEQL (Westall *et al.*, 1976) suggest that the solubility of $Ni(OH)_2(s)$ at the reaction conditions employed in this study is

TABLE 1
Nickel Loadings on the Pyrophyllite and Montmorillonite Components of the Standard Mixtures, and the Distribution of Ni over the Mixture Components[a]

	$Ni_{pyrophyllite}$				$Ni_{montmorillonite}$			
Standard mixture	Loading[b] (mg kg^{-1})	% of total[c]	[Solid][d] (g L^{-1})	$[Ni]_0$[e] (mM)	Loading[b] (mg kg^{-1})	% of total[c]	[Solid][d] (g L^{-1})	$[Ni]_0$[e] (mM)
(1)	6000	100	10.0	2.3	0	0	—	—
(2)	4000	67	22.5	2.3	2000	33	15.0	0.9
(3)	3000	50	35.2	2.3	3000	50	19.5	1.7
(4)	2000	33	60.1	2.3	4000	67	15.0	2.0
(5)	0	0	—	—	6000	100	10.0	2.3

[a] The Ni loading of each standard mixture was 3000 mg kg^{-1}, since the pyrophyllite and montmorillonite components were mixed in a 50%–50% (dry) weight ratio. Also given are the solid concentrations and the initial Ni concentrations that were used to prepare the mixture components.
[b] Ni loading on standard mixture component.
[c] Contribution (in %) of sorbed Ni on standard mixture component to total sorbed Ni in standard mixture.
[d] Solid concentration.
[e] Initial Ni concentration.

reached at a Ni concentration of 7.7 mM. Based on these calculations, our systems are undersaturated with respect to $Ni(OH)_2$(s) in all cases (initial Ni concentrations $\leq$2.3 mM). There is, however, a significant variation of reported log K_{sp} values for $Ni(OH)_2$(s) in the literature (-10.99 to -18.06; Mattigod *et al.* (15)), some of which would suggest oversaturation with respect to $Ni(OH)_2$(s) in our systems at the initial Ni concentrations used. A recent study by Mattigod *et al.* (15), investigating the solubility of $Ni(OH)_2$(s) as a function of pH and reaction time, showed that the Ni concentration in a supersaturated solution at pH 7.5 (in a 0.01 M $NaClO_4$ background) was $>$3 mM even after a reaction time of 90 days. Using XAFS, Scheidegger *et al.* (10) demonstrated that the Ni removal from solution in Ni/pyrophyllite and Ni/montmorillonite systems under identical reaction conditions as used in our study, was not due to $Ni(OH)_2$(s) formation in solution at any time during a 15 min to 3 month reaction time period. Based on these studies, we conclude that in our systems, Ni removal from solution is solely due to Ni sorption to the clay mineral surface, and not due the formation of $Ni(OH)_2$(s) in solution.

The wet pastes of the pyrophyllite and montmorillonite components of the standard mixtures were not mixed until about 5 min prior to XAFS analysis, and immediately submerged in liquid N_2 to avoid further reactions. The reacted mixture, which also had a total Ni loading of 3000 mg kg^{-1}, was prepared at an initial Ni concentration of 2.3 mM and a solid concentration of 34.7 g L^{-1}.

The Ni distributions (as % of total Ni) over the pyrophyllite and montmorillonite phases in the standard mixtures as given in Table 1 could also have been achieved by mixing pyrophyllite of e.g. 6000 mg kg^{-1} with appropriate amounts of e.g. 2000 mg kg^{-1} montmorillonite. It should be realized, however, that the intensities of the Ni–Ni/Al peak in the radial structure functions will be a function of two factors: (i) the distribution of Ni over the mixture components (surface precipitates on pyrophyllite, adsorbed species on montmorillonite); and (ii) the surface loading on the pyrophyllite phase. The first factor accounts for the "dilution" of the Ni–Ni/Al signal as a result of the presence of adsorbed species, which is due to the fact that XAFS provides an average bonding environment of total sorbed Ni. The second factor accounts for the structure of the surface precipitates at the pyrophyllite surface. The Ni–Ni/Al peak increases with increasing loading level, indicating the growth of precipitate clusters at the pyrophyllite surface with increasing Ni loading (10). By preparing the standard mixtures according to the procedure we used, both factors are accounted for, whereas the alternative procedure only accounts for the dilution effect.

The Ni sorption experiments were carried out in 0.1M $NaNO_3$, and at pH 7.5, maintained using a pH-stat apparatus. The reaction time was 40 min and the initial Ni concentrations were as given previously. Hydration of the clays was carried out in two steps. First, the clays were hydrated in background electrolyte for 24 h on a reciprocal shaker. Next, the suspension was brought to the desired solids concentration and placed on the pH-stat apparatus. The suspension was vigorously stirred with a magnetic stir bar and purged with N_2 to eliminate CO_2. The pH was maintained at pH 7.5 using 0.1 M NaOH. After 2 h, an appropriate amount of Ni from a 0.1 M $Ni(NO_3)_2$ stock solution was added in stepwise additions within a 3 min period to achieve the desired initial Ni concentration. After a reaction time of 40 min after the last Ni addition, the suspension was centrifuged and the supernatant was passed through a 0.2 μm membrane filter. The filtered supernatant was analyzed for Ni by atomic absorption spectrometry. The sorbed amount of Ni was calculated from the difference between initial and final Ni concentrations. Washing the remaining wet pastes to remove entrained electrolyte was not necessary since in all samples the amount of Ni sorbed at the mineral surface was at least 40

times higher than the amount of Ni in the entrained electrolyte. The samples were sealed and stored in a refrigerator to keep them moist for XAFS analysis.

XAFS spectra were recorded at Beamline X-11A of the National Synchroton Light Source, Brookhaven National Laboratory, Upton, NY. The electron storage ring operated at 2.5 GeV with an average beam current of 180 mA. A Si(111) crystal was employed in the monochromator with a sagittally focused beam. A 0.5 mm premonochromator slit width was used. The height of the entrance slit was readjusted as necessary to compensate for vertical motion of the stored electron beam. Higher order harmonics were suppressed by detuning 25% from the maximum beam intensity.

The beam energy was calibrated by assigning the first inflection on the K-absorption edge of a nickel metal foil to an energy of 8333 eV. The spectra were collected in fluorescence mode using a Lytle detector. The samples were placed at a 45° angle to the incident beam, and a wide-angle collector with the ionization chamber was located at 45° off the sample (i.e., 90° off the incident beam). Fill-gases used were N_2 for the Lytle detector and Ar for the I_0 detector. A Co filter and Soller slits were placed between the sample and the detector to reduce elastically scattered X-rays entering the fluorescence detector. The spectra were collected at 77 K to reduce damping of the XAFS oscillation by thermal disorder. The samples were packed into stainless steel sample holders, and mounted on a Cu cold finger that was connected to a liquid N_2 reservoir. To eliminate the possibility of an XAFS contribution from impurities in the sample holder, the sample holder was wrapped in Pb foil. To minimize the heat transfer imposed on the cold finger, samples were precooled by immersion into liquid N_2 for several min prior to analysis. Scans were collected in triplicate to improve the signal to noise ratio.

Background subtraction and Fourier filtering were accomplished with the program MacXAFS 4.0. The χ function was extracted from the raw data by using a linear pre-edge background and a spline post-edge background, and normalizing the edge to unity. The data were then converted from energy to k space and weighted by k^3 to compensate for the damping of the XAFS amplitude with increasing k. Structural parameters were extracted with fits to the standard EXAFS equation. *Ab initio* amplitude and phase functions for single shells were calculated using the FEFF6 code, in combination with ATOMS. Reference compounds used were β-$Ni(OH)_2$ (Johnson Mattey Co.) and takovite ($Ni_6Al_2(OH)_{16}CO_3 \cdot H_2O$; Kambalda W.A., Australia). The amplitude of the theoretical data was additionally adjusted by a factor determined from fits to the experimental data for the reference compounds. In all cases except standard mixture 5 (Table 1), multishell fitting was done in R space over the range ΔR = 1.07–3.12 Å with Δk = 3.2–13.6 $Å^{-1}$. For standard mixture (5), we used ΔR = 1.07–2.30 Å with Δk = 3.2–13.6 $Å^{-1}$. The smaller R range for this sample, where all the Ni is sorbed on the montmorillonite component, is due to the absence of a second shell in the radial structure function of this sample. The only constraint used in the fitting procedure was to fix the Debye–Waller factors of the Ni–Ni and Ni–Al shells at 0.005 $Å^2$. The R_{Ni-O} and R_{Ni-Ni} are estimated to be accurate to ±0.02 Å, and the N_{Ni-O} and N_{Ni-Ni} values are estimated to be accurate to ±20%. The estimated accuracies for N_{Ni-Al} and R_{Ni-Al} are ±60% and ±0.06 Å, respectively. The accuracy estimates are based on the results of theoretical fits to spectra of reference compounds of known structure. A discussion on the fitting procedure employed here and the accuracy estimates is given in Scheidegger *et al.* (10).

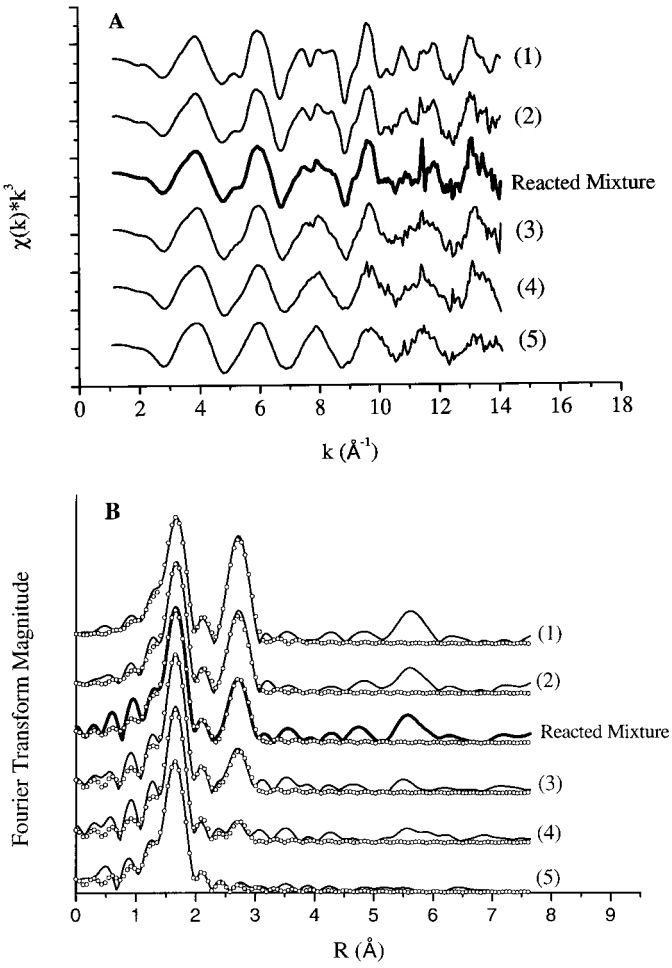

FIG. 2. (A) The k^3 weighted χ functions of the reacted mixture and the standard mixtures. The standard mixtures are numbered as in Table 1. (B) Comparison of the measured (solid lines) and the fitted (dotted lines) radial structure functions (uncorrected for phase shift) of the reacted mixture and the standard mixtures. For all radial structure functions, Fourier transformation was performed over Δk = 3.2 − 13.6 $Å^{-1}$. The standard mixtures are numbered as in Table 1.

RESULTS AND DISCUSSION

Figure 2 shows the k^3 weighted χ functions (Fig. 2a) and radial structure functions of the reacted mixture and the stan-

TABLE 2
Structural Parameters Derived from XAFS Analysis for the Reacted Mixture and the Standard Mixtures; The Standard Mixtures Are Numbered as in Table 1

	Ni–O			Ni–Ni			Ni–Al		
Mixture	N^a	R (Å)^b	σ^2 (Å^2)^c	N	R (Å)	σ^2 (Å^2)^d	N	R (Å)	σ^2 (Å^2)^d
(1)	6.2	2.05	0.0035	5.3	3.05	0.0050	2.9	3.05	0.0050
(2)	6.1	2.05	0.0032	3.0	3.05	0.0050	1.2	3.06	0.0050
Reacted mixture	6.1	2.05	0.0030	2.8	3.05	0.0050	1.2	3.12	0.0050
(3)	5.8	2.05	0.0025	2.4	3.04	0.0050	2.1	3.08	0.0050
(4)	5.7	2.05	0.0027	1.3	3.04	0.0050	1.6	3.09	0.0050
(5)	6.3	2.05	0.0033						

[a] Coordination number.
[b] Interatomic distance.
[c] Debye–Waller factor.
[d] The Debye–Waller factors of the Ni–Ni and Ni–Al shell were fixed at 0.0050 Å^2.

dard mixtures (Fig. 2b). The solid lines in Fig. 2b represent the Fourier transforms of the measured data, and the dotted lines those of the theoretical spectra derived with parameters from the fitting procedure. A good agreement between the Fourier transformed XAFS functions and the theoretical fits is observed.

Figure 2b shows that the intensity of the first (Ni–O) peak is the same for all mixtures. For the standard mixtures, the intensity of the second (Ni–Ni/Al) peak increases significantly with increasing fraction of Ni loading associated with the pyrophyllite component. The intensity of the second peak of the reacted mixture is smaller than that of standard mixture 2 (67% Ni on pyrophyllite), but larger than that of standard mixture 3 (50% Ni on pyrophyllite). This indicates that in the reacted mixture the amount of Ni sorbed on the pyrophyllite is between 50% and 67% of the total sorbed Ni. Figure 2 also shows peaks beyond the second shell at R = 5–6 Å. These result from multiple scattering among Ni atoms (8, 13), which was not characterized in the data analysis for this study.

In Table 2, the structural parameters derived from the XAFS data are presented. The coordination number N of a given shell is related to the intensity of the shell peak in the radial structure functions. The coordination number of the first shell ($N_{\text{Ni–O}}$) is about 6 for all samples, indicating that Ni is present in an octahedral environment, surrounded by 6 O atoms. The Ni–O bond distance (2.05 Å) is the same in all samples.

The fit results of the second coordination shell show that the number of second neighbor Ni atoms ($N_{\text{Ni–Ni}}$) increases with increasing fraction of Ni associated with the pyrophyllite phase in the standard mixtures. For the reacted mixture, 2.8 Ni atoms were fit in the second shell. As observed in the RSF's, this number falls between standard mixture 2 ($N_{\text{Ni–Ni}}$ = 3.0), and standard mixture 3 ($N_{\text{Ni–Ni}}$ = 2.4). The Ni–Ni bond distance (≈3.05 Å) is the same in all samples. No trend is observed in the $N_{\text{Ni–Al}}$ numbers of the third coordination shell, which also contributes to the second peak in the RSF's. However, the accuracy of $N_{\text{Ni–Al}}$ (±60%) is poor compared to $N_{\text{Ni–Ni}}$ (±20%).

We hypothesized that the intensity of the second Ni–Ni/Al peak in the RSF's can be used to estimate the distribution of Ni over the pyrophyllite and montmorillonite components in the reacted mixture. The intensity of the Ni–Ni/Al peak is reflected in the value of $N_{\text{Ni–Ni}}$ obtained from the theoretical fit of the XAFS data, and is a measure for the amount of Ni sorbed on the pyrophyllite component. Since the fractions of total Ni associated with the pyrophyllite component (%Ni$_{\text{pyrophyllite}}$) are known for the standard mixtures (Table 1), we plotted these values as a function of $N_{\text{Ni–Ni}}$ obtained from the theoretical fits to the XAFS data (Fig. 3). A linear relation between these variables is observed (%Ni$_{\text{pyrophyllite}}$ = 18.64$N_{\text{Ni–Ni}}$ + 5.26; R^2

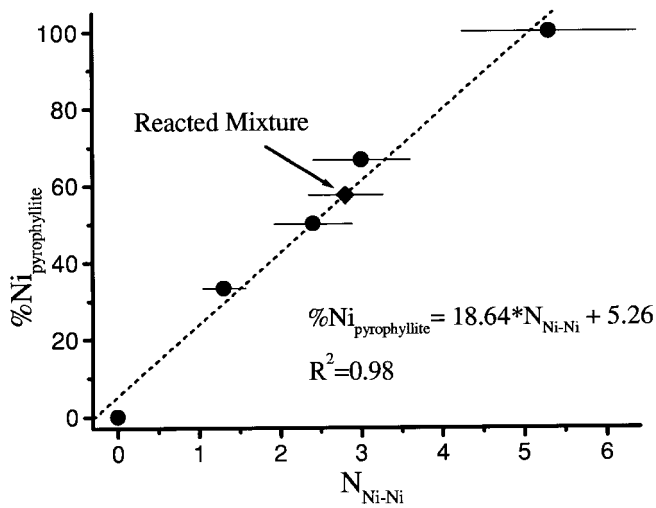

FIG. 3. Plot of the % of total sorbed Ni associated with the pyrophyllite component as a function of $N_{\text{Ni–Ni}}$ derived from XAFS analysis for the standard mixtures. The dashed line represents the best fit to the data. Error bars indicate the accuracy (±20%) of the $N_{\text{Ni–Ni}}$ coordination numbers derived from EXAFS data fitting.

TABLE 3

Regression Statistics of the Relation between $\%Ni_{pyrophyllite}$ and N_{Ni-Ni} Derived from the XAFS Results of the 5 Standard Mixtures

	Mean	Standard error	*p* level
Slope	18.64	1.40	0.0009
Intercept	5.26	4.10	0.30

$= 0.98$). The regression statistics of this equation are presented in Table 3. By applying this relation to the reacted mixture ($N_{Ni-Ni} = 2.8$; Table 2), the total Ni sorbed on the pyrophyllite component in the reacted mixture is estimated at $(57.5 \pm 8)\%$, where 57.5% is the mean and $\pm 8\%$ defines the 95% confidence interval of the estimate. This corresponds to a Ni loading of 3450 mg kg^{-1} (95% confidence interval: 2970–3930 mg kg^{-1}) on the pyrophyllite phase, and a Ni loading of 2550 mg kg^{-1} (95% confidence interval: 2070–3030 mg kg^{-1}) on the montmorillonite phase. Thus, the pyrophyllite component sorbs 1.4 times (95% confidence interval: 1.0–1.9) as much Ni as the montmorillonite component, which suggests that it is slightly more competitive for Ni uptake than the montmorillonite component in the reacted mixture under the reaction conditions used.

The initiation of surface precipitation on the pyrophyllite surface occurs at low surface loadings (<1500 mg kg^{-1}). However, since we used pyrophyllite samples with Ni loadings ≤ 6000 mg kg^{-1}, it is likely that also significant amounts of adsorbed Ni were present at the pyrophyllite surface. We were not able to distinguish between adsorbed Ni and Ni present in Ni/Al hydroxide precipitates at the pyrophyllite surface in our XAFS data. The Ni loading on the pyrophyllite phase of the reacted mixture was estimated to be 3450 mg kg^{-1}, which indicates that a substantial amount ($>55\%$) of total Ni sorbed on the pyrophyllite phase in the reacted mixture is in the form of surface precipitates. This suggests that the surface precipitation mechanism at the pyrophyllite surface is more effective for Ni uptake than the adsorption mechanism at the montmorillonite surface in the reacted mixture under the reaction conditions employed in this study.

For further evaluation of the Ni sorption behavior in our mixed system, we carried out two single mineral sorption studies, where montmorillonite and pyrophyllite were separately reacted under the same reaction conditions as the reacted mixture (0.1 M $NaNO_3$ background electrolyte; pH 7.5; reaction time = 40 min, initial Ni concentration = 2.3 mM), except for the solids concentration, which was 17.4 g L^{-1}. This solids concentration was used because it is half the total solids concentration of the 50–50 wt% reacted mixture, and thus equals the solids concentration of either mineral in the reacted mixture. Under these reaction conditions, pyrophyllite reaches a Ni loading level of 4728 mg kg^{-1}, and montmorillonite a Ni loading level of 3952 mg kg^{-1}. As expected, these loading levels are higher than the estimated loading levels on the pyrophyllite and montmorillonite surface in the reacted mixture (3450 and 2550 mg kg^{-1}, respectively) due to the absence of a competing surface in the singly reacted systems. By taking the ratio of Ni sorption on pyrophyllite to Ni sorption on montmorillonite for the singly reacted systems, it is found that singly reacted pyrophyllite sorbs 1.2 times as much Ni as singly reacted montmorillonite. In the reacted mixture, Ni sorption on pyrophyllite was estimated to be 1.4 times as high as Ni sorption on montmorillonite. The 95% confidence interval of this estimate is 1.0–1.9. The value of 1.2 calculated for the single clay mineral systems falls in this interval, indicating that there are no significant differences in this ratio between the singly reacted systems and the reacted mixture. This suggests that the affinity of Ni for the montmorillonite and pyrophyllite surface is similar in the reacted mixture and the single mineral systems. Nickel surface precipitation on the pyrophyllite phase is found to be more effective than Ni adsorption on the montmorillonite phase in the reacted mixture, which is consistent with the results from the single clay mineral systems. We conclude, therefore, that the mechanisms of adsorption on montmorillonite and surface precipitation on pyrophyllite are competing for Ni uptake in the reacted mixture, and that neither mechanism truly out-competes the other in the reaction time of 40 min employed in this study. Thus, when modeling Ni sorption results for systems similar to our pyrophyllite–montmorillonite mixture, both surface precipitation and adsorption should be considered. Over longer reaction times (time scales of days), surface precipitation is expected to occur on both the pyrophyllite and montmorillonite phase based on the results of Scheidegger *et al.* (10). At these longer reaction times, therefore, surface precipitation is expected to be the main mode of Ni uptake in the pyrophyllite–montmorillonite mixture.

CONCLUSIONS

In this study we were able to apply XAFS as a tool to distinguish sorption mechanisms on different clay minerals, and to estimate the distribution of Ni between the mineral phases in a 1:1 mixture of pyrophyllite and montmorillonite. The results suggest that the pyrophyllite component is more competitive for Ni uptake than the montmorillonite component. In terms of sorption mechanisms, this suggests that surface precipitation on the pyrophyllite phase is a more effective mechanism for Ni uptake than adsorption at the montmorillonite surface under the reaction conditions used in this study. The partitioning of Ni over the mixture components was found to be similar to what would be expected for single clay mineral sorption results for the mixture components, which indicated that both adsorption on montmorillonite and surface precipitation on pyrophyllite are important mechanisms for Ni uptake in the clay mixture during the reaction time of 40 min employed in this study.

ACKNOWLEDGMENTS

The authors are grateful to the USDA-NRICGP, the DuPont Co., and the State of Delaware for their support of this research. E.J.E. appreciates the receipt of a College of Agricultural and Natural Resources Competitive Graduate Fellowship. Thanks are also extended to Dr. A. M. Scheidegger for assistance with data analyses and to Drs. R. G. Ford, A. C. Scheinost, and D. G. Strawn for their critical comments on the manuscript.

REFERENCES

1. Sparks, D. L., "Environmental Soil Chemistry." Academic Press, San Diego, 1995.
2. Fendorf, S. E., Fendorf, M., Sparks, D. L., and Gronsky, R., *J. Colloid Interface Sci.* **153,** 37 (1992).
3. Fendorf, S. E., Sparks, D. L., Fendorf, M., and Gronsky, R., *J. Colloid Interface Sci.* **148,** 295 (1992).
4. Charlet, L., and Manceau, A., *Geochim. Cosmochim. Acta* **58,** 2577 (1994).
5. Fendorf, S. E., and Sparks, D. L., *Environ. Sci. Technol.* **28,** 290 (1994).
6. Junta, J. L., and Hochella, Jr., M. F., *Geochim. Cosmochim. Acta* **58,** 4985 (1994).
7. O'Day, P. A., Brown, G. E., Jr., and Parks, G. A., *Clays Clay Miner.* **42,** 337 (1994).
8. O'Day, P. A., Brown, G. E., Jr., and Parks, G. A., *J. Colloid Interface Sci.* **165,** 269 (1994).
9. Scheidegger, A. M., Lamble, G. M., and Sparks, D. L., *J. Colloid Interface Sci.* **186,** 118 (1997).
10. Scheidegger, A. M, Strawn, D. G., Lamble, G. L., and Sparks, D. L., *Geochim. Cosmochim. Acta.* **62,** 2233 (1998).
11. Fendorf, S. E., Lamble, G. M., Stapleton, M. G., Kelley, M. J., and Sparks, D. L., *Env. Sci. Technol.* **28,** 284 (1994).
12. Fendorf, S. E., and Fendorf, M., *Clays Clay Miner.* **44,** 220 (1996).
13. Papelis, C., and Hayes, K. F., *Colloids Surf. A: Physicochem. Eng. Aspects* **107,** 89 (1996).
14. Westall, J., Zachary, J. L., and Morel, F., Technical Note 18, Dept. of Civil Eng., MIT, Cambridge, MA, 1976.
15. Mattigod, S. V., Ray, D., Felmy, A. R., and Rao, L., *J. Solution. Chem.* **26,** 391 (1997).